Heliyon 8 (2022) e10102

Contents lists available at ScienceDirect

Heliyon

journal homepage: www.cell.com/heliyon

Research article

A combined study on structures and vibrational spectra of the antiviral rimantadine using SQMFF and DFT calculations

Maximiliano A. Iramain [a], José Ruiz Hidalgo [a], Tom Sundius [b], Silvia Antonia Brandán [a,*]

[a] Cátedra de Química General, Instituto de Química Inorgánica, Facultad de Bioquímica, Química y Farmacia, Universidad Nacional de Tucumán, Ayacucho 471 (4000), San Miguel de Tucumán, Tucumán, Argentina
[b] Department of Physics, University of Helsinki, Finland

GRAPHICAL ABSTRACT

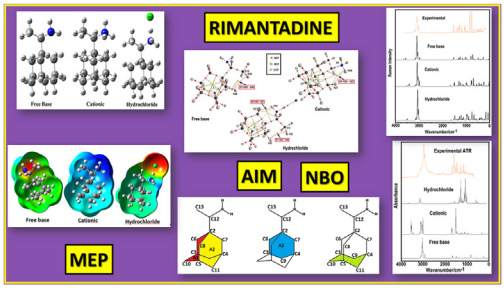

ARTICLE INFO

Keywords:
Rimantadine
Structural properties
Force fields
Vibrational analysis
DFT calculations

ABSTRACT

In this research, a combined study on structures and vibrational spectra of antiviral rimantadine have been performed using hybrid B3LYP/6–311++G** calculations and the scaled quantum force field (SQMFF) procedure. Harmonic force fields and scaled force constants of Free Base (FB), Cationic (CA) and Hydrochloride (HCl) species derived from the antiviral rimantadine have been calculated in gas phase and in aqueous solution using normal internal coordinates and scaling factors. Good correlations were acquired comparing the theoretical IR, Raman, ^{1}H– ^{13}C-NMR and UV spectra of three species with the analogous experimental ones, suggesting probably, the presence of all them in both phases. The main force constants of three species have evidenced lower values than the corresponding to antiviral amantadine. The ionic character of N1–H33···Cl36 bond of HCl species in aqueous solution evidence positive Mulliken charge on N1 atom indicating that this species is as CA one. Rimantadine presents higher solvation energies in water than other antiviral species, such as chloroquin, niclosamide, cidofovir and brincidofovir. The FB and HCl species of rimantadine are slightly less reactive than the corresponding to amantadine while the opposite is observed for the CA species. The predicted ECD spectra for the FB and CA species show positive Cotton effect different from the negative observed for the HCl one. These different behaviours of three species of rimantadine could probably explain the differences observed in the intensities of bands predicted in the electronic spectra of these species.

* Corresponding author.
E-mail address: sbrandan@fbqf.unt.edu.ar (S.A. Brandán).

https://doi.org/10.1016/j.heliyon.2022.e10102
Received 21 April 2022; Received in revised form 21 May 2022; Accepted 25 July 2022

1. Introduction

Vibrational studies of any species are essential to detect samples in different states using the infrared and Raman spectroscopies. This technique allows the rapid detection of a substance by using small amount of sample in an easy and reliable way and, in particular, the complete assignments can be performed when the DFT calculations are combined with the SQMFF approach and the vibrational spectra [1, 2, 3, 4, 5]. In this work, structures and vibrational studies of three derived species of rimantadine, an antiviral agent used to treat the influenza virus, were performed because, so far, the complete assignments of its FB, CA and HCl species are not reported yet [6, 7, 8, 9, 10, 11, 12, 13]. Recent studies on those three species of antiviral amantadine have revealed that the CA species presents higher solvation energy while positive Mulliken charge on N atom of HCl species in solution explained the ionic character of H···Cl bond [14]. On the other hand, HCl amantadine is the most reactive species in both media while the CA ones due to high gap values is the less reactive of species in the two media. This work was performed to know how the presence of an additional chiral C atom containing an activating and donor H bonds, CH_3 and NH_2 groups, respectively have influence on the properties of three species of rimantadine, as compared with amantadine [14]. The simplified three structures of rimantadine compared with the corresponding to amantadine are shown in the Scheme 1. The aims here are first, to optimize the structures of FB, CA and HCl forms of rimantadine in the two media using the B3LYP/6–311++G** level. Second, to predict its properties and reactivities in the two media and, to assign the experimental IR and Raman spectra using normal internal coordinates (NIC), scaling factors, the SQMFF procedure and the Molvib program [15, 16]. Then, comparisons of theoretical properties for all rimantadine species with reported for different antiviral agents, in particular, with amantadine are presented. These comparisons are interesting to analyse the influence of acceptors and donor's groups on their properties [14, 17, 18, 19]. Moreover, the correlations between the predicted ^{1}H- and ^{13}C-NMR spectra with the corresponding experimental ones allow to reproduce the theoretical optimized structures of three species of rimantadine. Finally, the electronic spectra were predicted for all species in aqueous medium at the same level of calculations, evidencing reasonable correlations when they are compared with the experimentally reported.

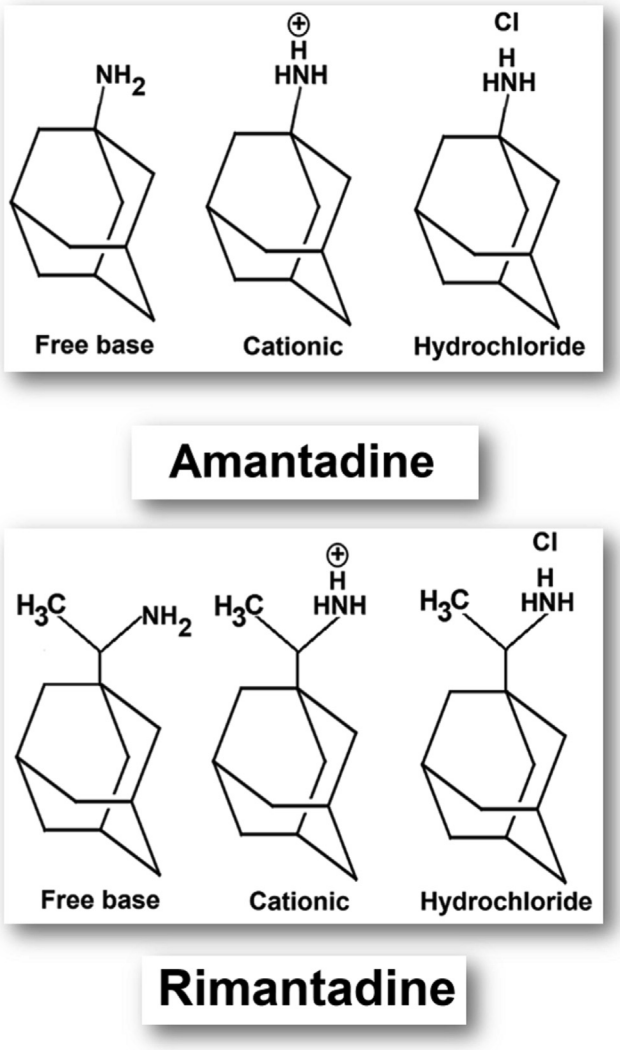

Scheme 1. Structures of free base, cationic and hydrochloride species of rimantadine compared with the corresponding to amantadine.

2. Material and methods

The modelled of three structures of rimantadine was carried out with the *GaussView* program [20] and, later optimized in the gas and aqueous solution phases with the functional hybrid B3LYP/6–311++G** and the Gaussian 09 program [21, 22, 23]. In solution, the solvation energies were calculated with the integral equation-formalism polarizable continuum model (IEF-PCM) and universal solvation method (SMD) [24, 25, 26] while the volume changes from the gas phase to solution were evaluated with the Moldraw program [27]. NBO 5.1 and AIM 2000 programs were employed to compute atomics charges, bond orders, main delocalization energies and topological properties while the Merz-Kollman charges and molecular electrostatic potentials were calculated according Besler et al. [28, 29, 30, 31]. The reactivities in both media were predicted from differences between the frontier orbitals known as gap, HOMO-LUMO. Then, the comportments of species in the two media were predicted calculating some descriptors, such as chemical potential (μ), electronegativity (χ), global hardness (η), global softness (S) and global electrophilicity index (ω) using typical equations [32, 33, 34, 35, 36, 37, 38]. The SQMFF approach, transferable scaling factors, NIC and the Molvib program were used to calculate the harmonic force fields of species in both media [5, 15, 16]. In the vibrational analyses, the symmetry of NH_2 group was considered C_{2v} while C_{3v} for the CH_3 and NH_3^+ groups. The definitions of three different axial rings in red, yellow and blue colours can be seen in Figure 1 (here, only for FB) while the equatorial one is observed in green colour. The ring in red colour is named A1, in yellow A2 and in blue colour A3. Then, the assignments of experimental IR and Raman bands of Rimantadine HCl in the solid phase [39] were made using Potential Energy Distribution (PED) contributions $\geq$ 10%. Corrections from activities to intensities were performed on all predicted Raman spectra by using equations proposed by Keresztury et al. in order to perform better correlations among them [40]. The ^{1}H and ^{13}C NMR chemical shifts were predicted in aqueous solution with the GIAO method [41]. After that, the UV-visible spectra of three structures in aqueous solution were predicted using the time-dependent DFT calculations (TD-DFT) [42, 43, 44, 45, 46] and, posteriorly compared with the corresponding experimental reported [47].

3. Results and discussion

3.1. Optimizations in different media

Optimized structures of three species of rimantadine with atoms labelling can be observed in Figure 2 while the calculated total uncorrected and corrected by zero-point vibrational energies (ZPVE), molecular volumes and dipole moments (μ) **with their corresponding** variations for the species of rimantadine in both phases by using the B3LYP/6–311++G** methods are shown in Table 1. Note that the HCl species in both media present the highest zero point vibrational energies (E_{ZPVE}) and the highest μ in aqueous solution while the FB species show

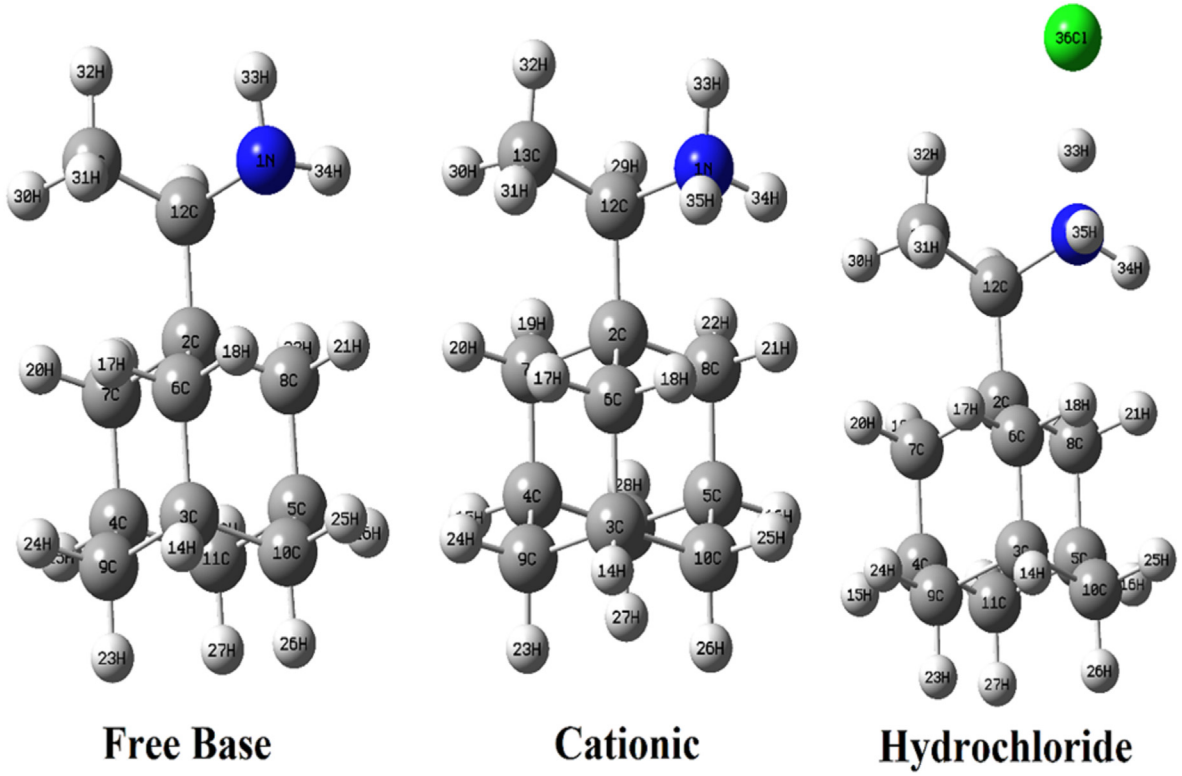

Figure 1. Definitions of rings for the three species of rimantadine.

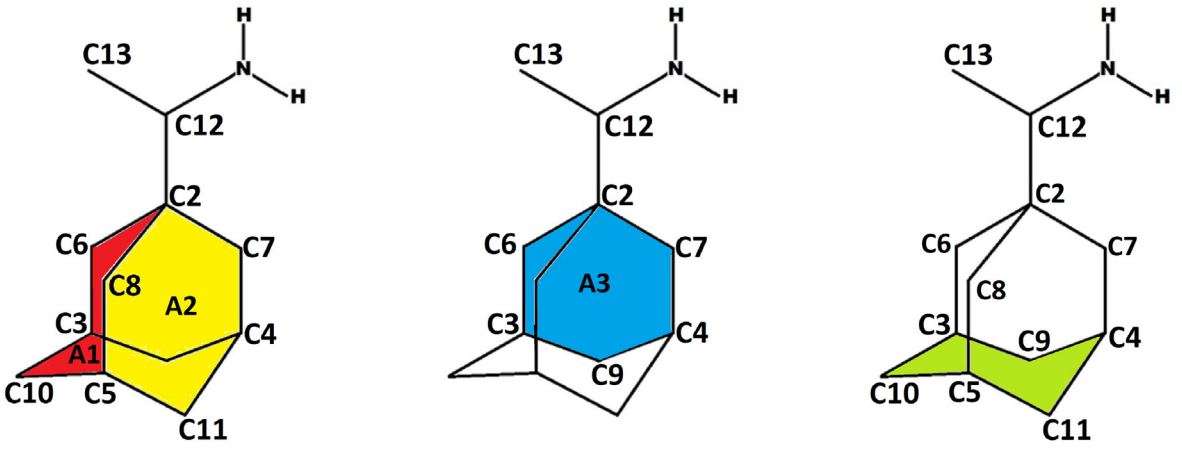

Figure 2. Structures of free base, cationic and hydrochloride species of rimantadine and atoms labelling.

Table 1. Calculated total energies (*E*), dipole moments (μ) and volumes (V) of three species of rimantadine in gas and aqueous solution phases.

B3LYP/6–311++G** Method					
Medium	E (Hartrees)	E_{ZPVE}	μ (D)	V (Å^3)	ΔV (Å^3)
Free base					
GAS	-524.8362	-524.5207	1.07	215.0	0.2
PCM	-524.8403	-524.5255	1.96	215.2	
Cationic					
GAS	-525.2118	-524.8816	9.63	218.8	1
PCM	-525.3105	-524.8806	13.33	217.8	
Hydrochloride					
GAS	-985.6901	-985.3635	9.59	244.8	0.9
PCM	-985.7279	-985.3980	14.87	245.7	

the smaller values in both properties. A very important result is that the HCl and CA species show practically the same variations of volume (1 Å^3) probably because they have similar μ in both media. Hence, the presences of NH_3^+ groups in both species justify the higher μ values in solution and, hence, its higher hydrations. Evaluating the calculated molecular volumes in the gas phase and its variations in aqueous solution it is possible to see slight increase of V for all species in solution, showing volume expansions in water. Then, observing the directions and orientations of μ vectors for the three species from Figure S1 we can see different orientations of μ vectors in the two media with the B3LYP/6–311++G** method. Obviously, the high μ values observed for both, CA and HCl species in aqueous solution support the higher hydrations of these two species with solvent molecules, due to the charged NH_3^+ groups. In the FB of rimantadine, the vector is located from centre in perpendicular direction to C2–C12 bond, the vector in the CA species is located from C2 in

direction toward NH_3^+ group, while the vector in the HCl species has its origins in C2 in the same direction of C2–C12 bond but towards outside. Note that the comparisons of μ vectors of three species of rimantadine with the corresponding to amantadine presented in Figure S1 show the same tendency and, where clearly the HCl species evidence changes in the orientations and directions of vectors due to Cl atoms. If now the solvation energies are computed for all species in aqueous solution, in Table 2 are given the uncorrected ($\Delta G_{un}^{\#}$) and corrected solvation (ΔG_c) energies taking in account the non-electrostatic terms but without consider the corrections by ZPVE. This correction was not possible to perform for the CA species of rimantadine because the value observed in solution (−524.8806 Hartrees) presents a lower value (−524.8816 Hartrees) than the corresponding in gas phase, as observed in Table 1 and as also was observed in amantadine [14]. The total non-electrostatic terms are obtained from the corresponding SMD calculations with the Gaussian program [23]. In the same Table 2 are compared the solvation energies for the three species of rimantadine with the reported for amantadine [14]. The ΔG_c values for FB and CA species of rimantadine are slightly lower than the corresponding to amantadine while the HCl species of rimantadine is a few higher than amantadine. These two antiviral agents present higher solvation energies in water than other antiviral species, such as chloroquin (−52.06 kJ/mol), niclosamide (−78, 43 kJ/mol), cidofovir (−169.21) and brincidofovir (−227.34 kJ/mol) [17, 18, 19]. Hence, we observed that brincidofovir presents a total of 15 groups (N–H and O–H groups and N and O atoms) in addition to the HPO_3 group and to a six member ring with a ΔG_c value of -227.34 kJ/mol. That value is slightly lower than the CA species of amantadine and rimantadine (−276.35 and -276.12 kJ/mol) which only present 3 N–H groups, one N atom and three six member's rings. Then, the fused six member's rings probably in the two antiviral amantadine and rimantadine play a very important role in the biological properties because both species evidence the same mechanisms of action, as descripted by De Clercq [6] but different from cidofovir and brincidofovir.

3.2. Geometrical parameters in both media

In Table 3 are presented the optimized parameters for the species of rimantadine in both media using the B3LYP/6–311++G** method compared with the corresponding experimental determined for the HCl form by using X-ray diffraction by Mishnev and Stepanovs [48]. These comparisons are presented by using the root-mean-square deviation values (RMSD). As expected, better correlations (lower RMSD) are observed for HCl in both media and the FB species, hence, analysing Table 3, the RMSD values for those two species are of 0.042 Å while for bond angles only for the HCl is observed the lower RMSD value (0.898–1.081°). In general, the dihedral N1–C12–C2–C6, N1–C12–C2–C7 and N1–C12–C2–C8 angles show good concordances. Besides, the RMSD values of bond lengths for both CA and HCl species decrease slightly in solution from 0.046–0.043 Å to 0.042–0.041 Å while the FB show RMSD of 0.042 Å in both media. A very interesting resulted is observed for the HCl species because the value of H33–Cl36 bond length in gas phase is 1.649 Å with a N–H–Cl bond angle of 176.6° while in solution that distance increases to 2.086 Å and the angle to 174.0°. Hence, the covalent character of H33–Cl36 bond in gas phase is transformed to ionic N1–H33···Cl36 in solution. Besides, in solution the bond angles for the CA and HCl species show lower RMSD values (1.019–1.081°), as it is expected because both compared species present NH_3 groups in its structures, as the experimental structure of rimantadine [48]. These results show that the theoretical optimized structures of three rimantadine species are appropriate to perform the vibrational studies and its corresponding assignments.

Table 2. Corrected and uncorrected solvation energies by the total non-electrostatic terms and by zero point vibrational energy (ZPVE) of three species of rimantadine in aqueous solution phases by using the B3LYP/6–311++G** method.

Rimantadine[a]			
Solvation energy (kJ/mol)			
Species	$\Delta G_{un}^{\#}$	ΔG_{ne}	ΔG_c
B3LYP/6–311++G** method			
Free base	-10.75	12.03	-22.78
Cationic	-258.90	17.22	-276.12
Hydrochloride	-99.15	17.18	-116.33
Amantadine[b]			
Solvation energy (kJ/mol)			
Species	$\Delta G_{un}^{\#}$	ΔG_{ne}	ΔG_c
B3LYP/6–311++G** method			
Free base	-15.21	7.86	-23.07
Cationic	-261.51	14.84	-276.35
Hydrochloride	-100.19	14.84	-115.03

[a] This work.
[b] From Ref [14].

3.3. Atomic charges, MEP and bond orders

In previous works on antivirals and alkaloids agents, the importance of studying atomic charges has been demonstrated and, in particular, in species charged as CA and HCl forms [1, 2, 3, 4, 14, 17, 18, 19]. Hence, for the species of rimantadine, the atomic Merz-Singh-Kollman (MK), Mulliken (MU) and natural population (NPA) charges were studied with the B3LYP/6–311++G** method in both media. We have compared three different types of charges, as suggested by Matta, because the Mu charges are totally basis set dependent [49]. These results for all atoms of three species are summarized in Table S1 but only the behaviours of those three charges for C and N atoms are presented in Figure S2 because these atoms present the higher variations. The exhaustive analyses of three graphics presented in Figure S2 show that the MK and MU charges present similar behaviours but different from NPA charges. In general, the NPA charges on all C and N atoms in the three species have negative charges evidencing the less negative values on C2 and C12 atoms, both linked between them, the first atom to rings and the second one to $H_2N–CH–CH_3$ moieties. The MU charges on N1 of HCl species in aqueous solution show a positive value (red circles on Figure S2) while in the FB and CA species the N atoms present negative values. Such observation in the HCl species could be probably justified by the conversion of covalent character of H33–Cl36 bond in gas phase to ionic N1–H33··· Cl36 bond in solution, as was evidenced in the antiviral amantadine [14]. On the other side, the MK charges on C12 atoms in all species present positive values (blue circles) while the three charges on the C13 atoms show negative values in all species of rimantadine but low values in the MK charges and most negative values in the MU charges. A very important observation can be seen in the MU charges on C8 atoms (see brown arrows) because in the FB its value is practically the same than C7 but in the CA and HCl species the values became less negative due to the influence of NH_3^+ groups. Table S1 shows that the MU and MK charges on all C atoms of CA and HCl species in both media have practically similar values, and only few modifications in the charges of FB species in both media are observed.

The MEP and the bond orders, expressed as Wiberg indexes for the three species of rimantadine in both media have been also studied at the same level of theory and the results can be seen in Table S2. Analysing deeply the results, for the FB in the two media are observed practically the same MEP values while slight differences can be seen on the atoms of CA and HCl species. However, the different colours on the mapped MEP surfaces graphed with the *GaussView* program suggest different concentrations of charges in the three species [20]. Hence, different regions of reactivity on the mapped MEP surfaces by red, blue and green colorations are evidenced, as it is given in Figure S3. Thus, the three colours are observed on the mapped MEP surfaces of FB and HCl species but different

Table 3. Comparison of calculated geometrical parameters for the free base, cationic and hydrochloride species of rimantadine in gas and aqueous solution phases compared with the corresponding experimental ones.

Parameters	B3LYP/6–311++G**[a]						Exp[b]
	Free base		Cationic		Hydrochloride		
	Gas	PCM	Gas	PCM	Gas	PCM	
Bond lengths (Å)							
N1–C12	1.475	1.482	1.546	1.521	1.500	1.515	1.475
C12–C13	1.532	1.530	1.524	1.525	1.529	1.525	1.521
C2–C12	1.559	1.556	1.549	1.550	1.554	1.550	1.532
C2–C8	1.552	1.552	1.554	1.552	1.552	1.553	1.520
C2–C7	1.550	1.551	1.553	1.552	1.551	1.550	1.502
C2–C6	1.547	1.547	1.549	1.548	1.549	1.549	1.510
C8–C5	1.541	1.541	1.543	1.541	1.541	1.540	1.527
C5–C11	1.539	1.539	1.539	1.539	1.539	1.539	1.489
C11–C4	1.539	1.539	1.539	1.539	1.539	1.539	1.479
C4–C7	1.542	1.541	1.542	1.541	1.541	1.541	1.549
C4–C9	1.541	1.540	1.540	1.540	1.541	1.540	1.533
C9–C3	1.541	1.541	1.540	1.540	1.541	1.540	1.504
C3–C6	1.543	1.543	1.546	1.544	1.543	1.543	1.520
C3–C10	1.540	1.540	1.540	1.540	1.540	1.541	1.458
C10–C5	1.541	1.540	1.540	1.540	1.541	1.540	1.466
RMSD[b]	**0.042**	**0.042**	**0.046**	**0.043**	**0.042**	**0.042**	
Bond angles (º)							
N1–C12–C13	107.4	107.6	106.8	106.8	106.7	107.2	106.2
N1–C12–C2	110.7	111.5	109.1	110.8	112.8	110.8	113.2
C13–C12–C2	114.7	114.9	118.0	117.0	116.7	117.0	116.4
C12–C2–C6	112.6	113.2	113.0	113.1	113.1	113.1	114.3
C12–C2–C7	110.2	109.7	108.2	108.2	109.1	109.1	108.3
C12–C2–C8	109.5	109.6	110.0	110.8	110.1	109.5	110.3
C2–C6–C3	110.5	110.6	110.0	110.2	110.4	110.2	110.9
C6–C3–C9	109.5	109.5	109.3	109.4	109.5	109.6	108.4
C6–C3–C10	109.8	109.7	109.6	109.8	109.6	109.6	111.4
C3–C9–C4	109.4	109.4	109.4	109.4	109.4	109.3	107.6
C3–C10–C5	109.3	109.4	109.5	109.4	109.4	109.4	110.1
C2–C7–C4	111.0	111.1	110.3	110.6	110.9	110.7	110.7
C7–C4–C9	109.3	109.2	109.1	109.3	109.1	109.2	108.7
C7–C4–C11	109.6	109.6	109.6	109.6	109.7	109.8	108.2
C11–C4–C9	109.4	109.4	109.8	109.5	109.6	109.5	110.1
C2–C8–C5	111.2	111.2	110.6	110.8	111.1	110.8	110.4
C8–C5–C10	109.0	109.1	109.1	109.1	109.2	109.3	109.6
C8–C5–C11	109.6	109.6	109.2	109.6	109.4	109.4	109.5
C5–C11–C4	109.2	109.1	109.2	109.1	109.1	109.1	110.4
C10–C3–C9	109.2	109.2	109.6	109.3	109.4	109.3	110.3
C10–C5–C11	109.6	109.5	109.9	109.6	109.6	109.6	109.4
RMSD[b]	**1.237**	**1.099**	**1.289**	**1.019**	**0.898**	**1.081**	
Dihedral angles (º)							
N1–C12–C2–C6	63.75	62.69	62.17	66.49	62.26	55.67	47.6
N1–C12–C2–C7	-174.87	-176.20	-177.44	-173.16	-177.00	-176.52	72.2
N1–C12–C2–C8	-46.69	-58.39	-59.74	-55.48	-59.15	-65.81	-66.4
RMSD[b]	**61.07**	**60.85**	**61.46**	**59.63**	**61.20**	**60.41**	

RMSD values in letter bold.
[a] This work.
[b] Ref [36].

from the CA one. This way, the FB shows strong red colour on the lone pairs of N1 atom and light blue colours on the H27 and H28 atoms of NH_2 group while in the HCl species the strong red colour on the Cl atom is observed while the strong blue colours on the three H atoms of NH_3 group. On the other hand, the CA species is positively charged and show blue colours on the entire surface with a high molecular electrostatic potential value (−0.20 a. u.). Thus, nucleophilic and electrophilic sites are characterized by red and blue colours, respectively where the potential reactions with potential biological electrophiles or nucleophiles take place while the green regions are inert sites. As in amantadine, different reaction sites are evidenced in the three species of rimantadine.

The bond orders (BO) totals by atom expressed, as Wiberg indexes for the three species of rimantadine have been computed with the NBO program and the 6–311++G** method [28]. In Table S2 are presented

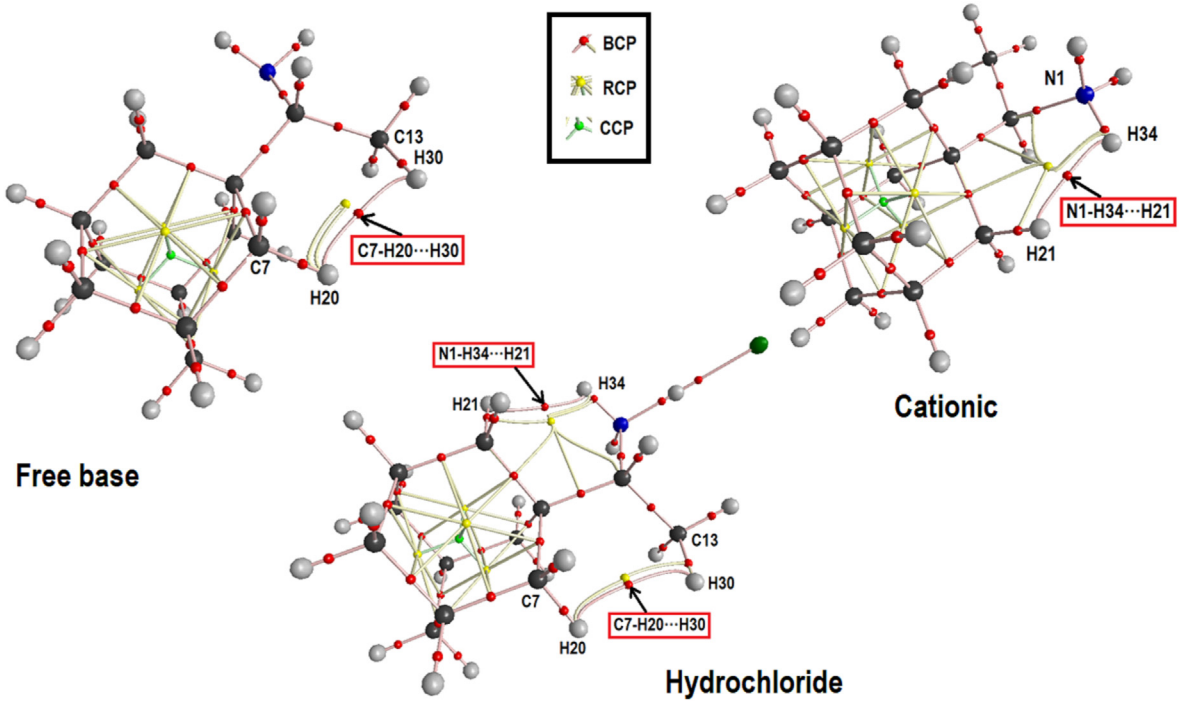

Figure 3. Molecular graphics of three species of rimantadine in gas phase showing their H bonds interactions by using the B3LYP/6–311++G** method.

these results for the three species. In general, the BOs of the three species of rimantadine no present significant differences in both media, while for the CA and HCl species few changes are observed. However, the Wiberg bond index matrix in the Natural Atomic Orbital (NAO) basis for the H33–Cl36 bond shows a covalent character in the HCl species in gas phase (0.255) which change to ionic in solution (N1–H33··· Cl36) with a value of 0.142. In amantadine, the covalent character of H29–Cl30 bond for the HCl species change of 0.355 in gas phase to ionic in solution (N1–H29··· Cl30) with a value of 0.123 [14]. Hence, the performed change is higher in amantadine.

3.4. Delocalization energies and topological properties

In pharmacological drug, the presence of acceptors and donors groups are important to estimate its solubility, permeability and oral bioavailability, as advised by Veber et al and Lipinski et al [50, 51]. Also, the existence of those groups can have influence on the stabilities of species and, for these reasons, delocalization energies and topological studies were predicted for the three species of rimantadine in both media using different NBO and AIM calculations [28, 29, 30]. First, the NBO program was used to compute the donor-acceptor energy interactions, expressed as E (2), by using Second-Order Perturbation Theory Analysis of Fock Matrix in NBO Basis [28]. Intra-molecular interactions are expected in the three species of rimantadine due to the presence of N–H bonds and N atoms (NH_2 and NH_3 groups), especially in solution. The main delocalization energies for all species of rimantadine are shown in Table S3 while a summary of total observed is presented in Table 4. Only two $\sigma \rightarrow \sigma^*$ and $LP \rightarrow \sigma^*$ transitions are observed for the FB and HCl species while for the CA only $\sigma \rightarrow \sigma^*$ transitions are observed in both media. Thus, higher energy values are expected for the HCl species in both media while the FB species present low total energies values, especially in gas phase and the lowest values are observed for the CA species in both media. Hence, the higher energy value observed for the HCl species in gas phase (1134.83 kJ/mol) indicates that this species is the most stable decreasing its stability in solution to 606.18 kJ/mol. On the contrary, the low values of CA species probably suggest high hydration in solution, as supported by its higher solvation energy, as also was observed for amantadine [14].

Table 4. Main delocalization energies (in kJ/mol) for the three species of rimantadine in gas and aqueous solution phases by using B3LYP/6–311++G** calculations.

Delocalization	B3LYP/6–311++G**					
	Free Base		Cationic		Hydrochloride	
	Gas	Water	Gas	Water	Gas	Water
$\Delta E_{\sigma \rightarrow \sigma^*}$	415.16	440.15	58.36	58.63	479.78	470.04
$\Delta E_{LP \rightarrow \sigma^*}$	29.26	27.50			655.05	136.14
ΔE_{TOTAL}	**444.42**	**467.65**	**58.36**	**58.63**	**1134.83**	**606.18**

An additional practical and useful tool to predict intra-molecular, H bonds, ionic, covalent polar, etc. interactions is the methodology based in the Bader's theory of atoms molecules where the topological properties are calculated by using the version 2000 of AIM program [29, 30]. Thus, for all species of rimantadine the electron density, $\rho\ (r)$, the Laplacian values, $\nabla^2\rho(r)$ and the $|\lambda 1|/\lambda 3$ ratio are calculated in the bond critical points (BCPs) and in the ring critical points (RCPs). Those parameters calculated with the B3LYP/6–311++G** method together with the distances of new H bonds for the three species in both media are shown in Table S4. The $|\lambda 1|/\lambda 3$ ratios are computed knowing the eigenvalues of the Hessian matrix $(\lambda 1, \lambda 2, \lambda 3)$. In the three species are observed the cage critical points (CCPs) because several rings form a cage characterized by green colours. The ionic or highly polar covalent interactions present $\lambda 1/\lambda 3 < 1$ and $\nabla^2\rho(r) > 0$ (closed-shell interaction) while the eigenvalues of the Hessian matrix in the CCPs have in the three species positive signs with similar values in the two media. Figure 3 displays the molecular structures of three species in gas phase showing H bonds interactions, BCPs, RCPs and CCPs. In Table 5 are summarized analyses of topological properties in the CCPs for the three species of rimantadine in gas and aqueous solution by using the B3LYP/6–311++G** method and in the BCPs for the HCl species in both media. Evaluating the results, we observed that the HCl form in gas phase and the FB and CA species in aqueous solution shows two new H bonds, as observed in Table S4. In the HCl species the C7–H20···H30 interaction disappear in solution while the bond distances of N1–H34·· H21 interactions in both media show for this species similar values although the value is higher in solution. On the

Table 5. Analysis of topological properties in the Cage critical point (CCPs) for the three species of rimantadine in gas and aqueous solution by using the B3LYP/6–311++G** method and in the Bond Critical Points (BCPs) for the hydrochloride species in both media.

B3LYP/6–311++G** Method								
Parameter[#]	Cage critical point						BCP	
	Free base		Cationic		Hydrochloride		H33···Cl36	H33···Cl36
	Gas	PCM	Gas	PCM	Gas	PCM	Gas	PCM
ρ(r)	0.0118	0.0119	0.0119	0.0119	0.0119	0.0119	0.0987	0.0365
$\nabla^2\rho(r)$	0.0728	0.0728	0.0728	0.7280	0.0728	0.0728	-0.0228	0.0564
λ1	0.0236	0.0236	0.0238	0.0239	0.0237	0.0238	-0.1821	-0.0463
λ2	0.0244	0.0244	0.0244	0.0245	0.0244	0.0246	-0.1820	-0.0463
λ3	0.0247	0.0247	0.0245	0.0246	0.0246	0.0246	0.3412	0.1491
$\|\lambda1\|/\lambda3$	0.9555	0.9555	0.9714	0.9715	0.9634	0.9675	0.5337	0.3103
Distances							1.6495	2.0864

[#] Parameters in a. u., Distances in Å

other hand, the CA species in solution and the HCl in both media show similar values of electron density. The strong N1–H33···Cl36 interaction in the HCl species justifies the higher stability of this species in both media, having in solution the following values: $\rho\ (r) = 0.0365$, $\nabla^2\rho(r) = 0.0564$ and $|\lambda1|/\lambda3$ ratio = 0.3103 (see Table 5). The transformation of covalent character of H33–Cl36 bond to ionic in the HCl species is clearly detected by the longer distance of bond in solution, as supported by BO studies and, as observed in Table 5. This resulted is the expected taking into account that the HCl species is a salt and, therefore, in solution it is in its CA form, as in the species of scopolamine and promethazine [1, 3].

3.5. Frontier orbitals and global descriptors

Parr and Pearson have suggested that the reactivity of a species can be calculated from the differences between the frontier orbitals calling this gap parameter [33, 36, 37, 38]. Thus, these gap values have been predicted for all species of rimantadine in both media using the hybrid B3LYP/6–311++G** method. Then, the behaviours of all species were evaluated in both media with some descriptors by using the gap values such as, the chemical potential (μ), electronegativity (χ), global hardness (η), global softness (S) and global electrophilicity index (ω). These descriptors are computed using known equations and that hybrid level of theory [32, 33, 34, 35, 36, 37, 38]. The calculated gap values and descriptors for the species of rimantadine in both media can be seen in Table S5. In the same table are presented the values for the antiviral amantadine. The lowest gap values for the HCl species of rimantadine in both media suggest its higher reactivities (5.4036 and 4.1890 eV) while the high gap values for the FB and CA species in both media suggest low reactivities. The behaviour of descriptors for the three species in the two media are presented in Figure S4. The figure suggests that the low reactivities of CA species in both media could be attributed to high electrophilicity indexes predicted and to lower μ values. The FB and the HCl species show practically the same behaviours in both media. Comparisons of descriptors predicted for rimantadine with reported for antiviral agents show in Table S6. From Table S5 is possible to see that the FB and HCl species of amantadine are slightly more reactive than those of rimantadine while the opposite is observed for the CA species.

3.6. Vibrational analyses

Hybrid B3LYP/6–311++G** calculations have optimized the three structures of rimantadine with C_1 symmetries and, taking into account the numbers of atoms present in FB, CA and HCl species are expected 96, 99 and 102 normal vibration modes, respectively. In the analysis of normal internal coordinates, C_{2v} and C_{3v} symmetries were considered for the NH_2 group of FB and NH_3^+ groups of CA and HCl groups. Here, the building of normal internal coordinates was similar to amantadine and, only the A1, A2 and A3 rings in axial position (vertical) were considered, as observed in Figure 1 [14]. The experimental Attenuated total reflectance infrared spectrum of HCl species of rimantadine in the solid state is given in Figure 4 compared with the corresponding predicted for the three species, in gas phase, by using the hybrid B3LYP/6–311++G** method [39]. Note that only the CA species of rimantadine shows two IR bands in the 1600-1500 cm^{-1} region with the same characteristic that experimental one, one of them weak and the other one strong at 1591 and 1576 cm^{-1}, respectively while the predicted IR spectrum of HCl species presents two strong IR bands at 783 and 674 cm^{-1}, as observed experimentally (771 and 696 cm^{-1}). In the

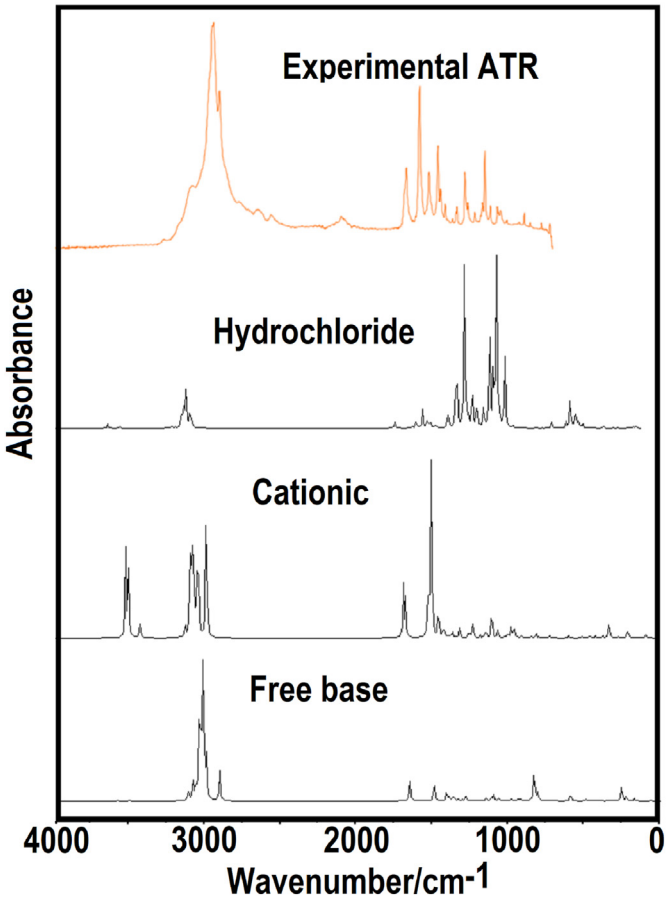

Figure 4. Experimental available Infrared spectra of free base and hydrochloride species of rimantadine in solid phase [1, 33, 34] compared with the predicted in gas phase for the three species by using the hybrid B3LYP/6–311++G** method.

IR spectrum of FB only presents strong bands at higher wavenumbers, as observed in the experimental spectrum. Hence, we can conclude that apparently the three species of rimantadine are present in the solid phase. In Figure 5 are compared the experimental and the predicted Raman spectra for the three species of rimantadine in gas phase at room temperature and at the same level of theory [39]. Better correlations among the Raman spectra are observed when the predicted spectra in activities for the three species of rimantadine are transformed to intensities by using equations reported [40]. We can say that due to the similarity between the predicted Raman spectra to experimental one the three species of rimantadine could be present in the solid phase. The harmonic force fields for all species were computed with the SQMFF procedure and the Molvib program employing the same level of theory and using transferable scale factors [17] and the normal internal coordinates. Then, the vibrational assignments were performed for the three forms of rimantadine using the scaled force fields and potential energy distribution (PED) contributions higher or equal to 10%. The observed and calculated wavenumbers and assignments for the three species in gas phase are summarized in Table 6. Analyses and discussions of assignments for the main groups are presented by regions.

3.6.1. Band assignments

4000-2000 cm^{-1} region. This region is characteristic of NH_2, NH_3, CH_3, CH_2 and C–H stretching modes of three species [1, 2, 3, 4, 14, 17, 18, 19]. Hence, the weak IR band at 3232 cm^{-1} is associated to the two NH_2 stretching modes of FB and to the three vibration NH_3 modes of CA and HCl species, as detailed in Table 6. In the HCl species, one of two NH_3 anti-symmetric modes and the symmetric mode are assigned at 3232 cm^{-1} but the other anti-symmetric mode is predicted by SQM calculations coupled with other modes between 976 and 866 cm^{-1} (see Table 6). In amantadine was also observed a similar situation because one N–H bond is linked to Cl atom of the HCl species [14]. Two CH_3 stretching modes in the three species of rimantadine are expected and assigned in approximately the identical regions but in the FB and HCl species the symmetric modes are predicted different from CA species, hence, they are assigned in different positions, as summarized in Table 6. The strong Raman bands at 2917, 2889 and 2849 cm^{-1} are associated respectively to symmetric modes of CH_3 and CH_2 of three species, as shown in Table 6. The group of weak IR bands at c. a. 2700 cm^{-1} could be assigned to combination's bands of some intense bands, for instance, 1508 + 1205 = 2713 cm^{-1}.

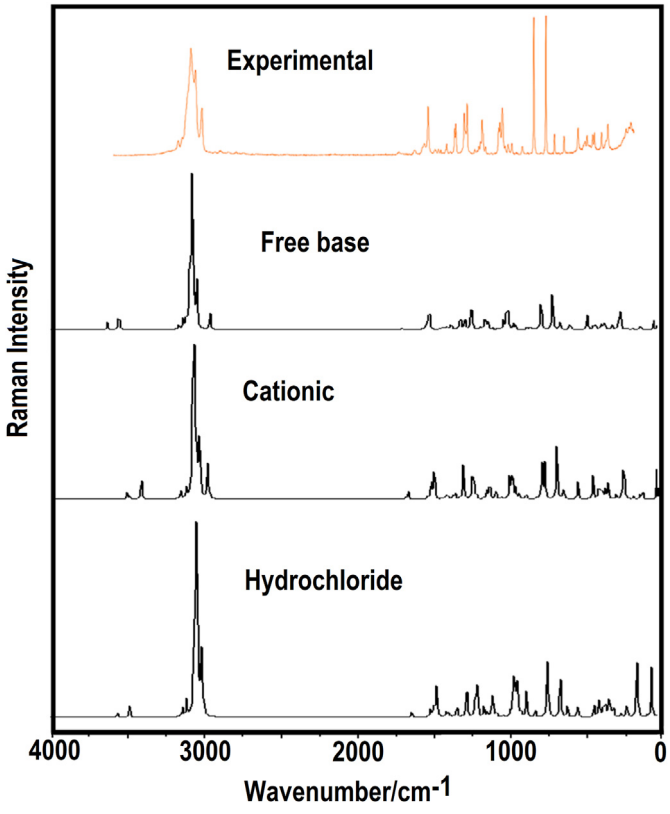

Figure 5. Experimental available Raman spectrum of hydrochloride species of rimantadine in solid phase [39] compared with the predicted in gas phase for the three species by using the hybrid B3LYP/6–311++G** method.

1800-1000 cm^{-1} region. The deformation, wagging and rocking modes of NH_2, NH_3, CH_3, CH_2 and C–H groups are expected in this region [1, 2, 3, 4, 14, 17, 18, 19]. The IR band at 1603 cm^{-1} is attributed to NH_2 deformation mode of FB and to an anti-symmetric mode of NH_3 group of the CA species while the strong IR band at 1508 cm^{-1} is assigned to other anti-symmetric mode of that group of CA species and to one anti-symmetric mode of same group of the HCl species. Due to Cl atom in the latter species, the other two expected NH_3 modes are predicted in different positions, thus, they can be assigned at 1435, 1357 and 1141 cm^{-1}. In the three species, the bands between 1455 cm^{-1} and 1408 cm^{-1} are related to the CH_2 deformations modes while the wagging and rocking modes are assigned between 1371/1314 and 1282/1106 cm^{-1} [1, 2, 3, 4,14,17,18, 19]. In the three species, some C–C stretching modes are predicted in this region from 1119 up to 976 cm^{-1} and some torsion rings modes are also observed in this region coupled with other modes between 1318 and 919 cm^{-1}.

1000-150 cm^{-1} region. Skeletal modes, such as NH_3 rocking modes, C12–N1, C12–C13 and C2–C12 stretching modes are assigned in this region, in addition to the deformations and torsion rings corresponding to the three species and to the three rings. As observed in amantadine, the C12–N1 stretching modes were predicted in different positions, thus, this mode in the three species is predicted at 821, 756 and 817 cm^{-1}, respectively. Evidently, the charge on N1 in the CA species has influence on C12–N1 bond and, hence, on the stretching mode. In the three species of rimantadine, as in amantadine, the deformations and torsions rings are predicted coupled among them, as observed in Table 6.

Comparing the vibrational assignments of the three species of rimantadine, with the corresponding to amantadine, we observed that the incorporation of C12 and CH_3 groups in rimantadine, modify slightly the positions of stretching and deformation modes of NH_2 of FB and of NH_3^+ groups of CA and HCl species. Although the higher changes between 1220 and 30 cm^{-1} are observed, specifically in the frequencies of wagging, rocking and twisting modes of those groups observed.

4. Force constants

The harmonic scaled force constants of three species of rimantadine have been computed in both media with the corresponding force fields using the SQMFF methodology [5, 15] and the Molvib program at the 6–311++G** level of theory [16]. These scaled force constants in gas phase are compared in Table 7 with the corresponding to amantadine. Evaluating first the results for the three species of rimantadine, we observed differences in the *f(νN-H)* force constants, as expected because in the FB these constants correspond to NH_2 group while they correspond to NH_3 groups in the other ones. The low value in the HCl species is due to Cl atom because form the larger H33···Cl36 bond. In relation to the *f(νC-N)* force constants we observed that for the CA species the value is low due to that the C12–N1 bond is longer (1.546 Å) than the corresponding to the FB and HCl species (1.475 and 1.500 Å, respectively) (see Table 3). The other force constants present practically similar values in the three species. Comparing the constants of rimantadine with amantadine, we observed that the incorporation of C12 and CH_3 groups in rimantadine, modify slightly the bond N–H bonds and angles of NH_2 of FB and of NH_3^+ groups of CA and HCl species and, hence, the related force constants. Note that practically all force constants values shown in Table 7 are higher in amantadine than rimantadine.

Table 6. Observed and calculated wavenumbers (cm^{-1}) and assignments for free base, cationic and hydrochloride species of rimantadine in gas phase by using B3LYP/6–311++G** calculations.

Experimental[c]		SQM[b]	Free base	SQM[b]	Cationic	SQM[b]	Hydrochloride
IR	Ra		Assignment[a]		Assignment[a]		Assignment[a]
3232w		3435	ν_aNH_2	3353	ν_aNH_3	3405	ν_aNH_3
3232w		3363	ν_sNH_2	3335	ν_aNH_3	3331	ν_sNH_3, ν_aNH_3
3232w				3262	ν_sNH_3		
3041m	2997w	2988	ν_aCH_3	3012	ν_aCH_3	3000	ν_aCH_3
2969sh	2969w	2959	ν_aCH_3	2977	ν_aCH_3	2974	ν_aCH_3
		2942	ν_aCH_2(C6)	2944	ν_aCH_2(C11)		
				2940	ν_aCH_2(C7)		
				2938	ν_aCH_2(C10)		
	2937sh			2937	ν_aCH_2(C9)	2936	ν_aCH_2(C7)
				2936	νC12-H29	2926	ν_aCH_2(C6)
				2930	νC3-H14, νC4-H15	2925	ν_aCH_2(C10)
				2928	νC4-H15	2920	νC12-H29
		2924	ν_aCH_2(C8)	2926	νC5-H16	2919	ν_aCH_2(C11)
2921sh		2921	ν_aCH_2(C7)			2918	ν_aCH_2(C9)
	2917vs	2917	ν_aCH_2(C10)	2923	νC3-H14	2913	νC5-H16
	2917vs	2912	ν_aCH_2(C11)	2916	ν_sCH_3	2909	ν_aCH_2(C8)
		2911	ν_aCH_2(C9)			2907	νC4-H15
2901sh	2909sh	2907	νC3-H14	2902	ν_sCH_2(C11),ν_aCH_2(C8)	2906	νC3-H14
		2903	ν_sCH_3	2900	ν_sCH_2(C9)	2906	ν_sCH_3
2893vs	2889s	2899	νC4-H15	2899	ν_sCH_2(C11),ν_sCH_2(C9)	2887	ν_sCH_2(C7)
2893vs	2889s	2896	νC5-H16	2890	ν_sCH_2(C7)	2885	ν_sCH_2(C11)
2893vs	2889s	2891	ν_sCH_2(C6)	2890	ν_sCH_2(C10)	2884	ν_sCH_2(C10)
	2885sh	2878	ν_sCH_2(C9)			2884	ν_sCH_2(C9)
		2878	ν_sCH_2(C10)				
2878sh	2877sh	2877	ν_sCH_2(C11)				
		2876	ν_sCH_2(C7)			2875	ν_sCH_2(C6)
		2870	ν_sCH_2(C8)	2845	ν_sCH_2(C6),ν_aCH_2(C6)	2866	ν_sCH_2(C8)
2854s	2849m	2792	νC12-H29	2834	ν_sCH_2(C8)		
2726w	2734w		1508 + 1205 = 2713		1191 + 1520 = 2711		2x1385 = 2770
1603m	1615w	1583	δNH_2	1591	δ_aNH_3		
1508s	1520w			1576	δ_aNH_3	1567	δ_aNH_3
1449m	1457w	1455	δCH_2(C6), $\delta CH_{2(C8)}$			1452	δ_aCH_3
				1451	δCH_2(C9), δCH_2(C11)	1450	δCH_2(C7), δCH_2(C6)
1440sh	1439sh	1443	δ_aCH_3	1440	δ_aCH_3	1439	δ_aCH_3
	1435m	1436	δCH_2(C6)	1434	δ_aCH_3	1435	δ_aNH_3
	1435m	1432	δCH_2(C6), δCH_2(C8)	1430	δCH_2(C9)	1430	δCH_2(C6), δCH_2(C11)
	1428sh	1431	δCH_2(C8)	1430	δCH_2(C11)	1429	δCH_2(C10),δCH_2(C7)
	1424sh	1430	δCH_2(C10),δ_aCH_3 $\delta CH_{2(C7)}$	1428	δCH_2(C10)	1427	δCH_2(C9)
	1418sh	1419	δCH_2(C11)	1415	δCH_2(C7), δCH_2(C6)	1417	δCH_2(C6), δCH_2(C11)
		1417	δCH_2(C9)	1414	δ_sNH_3	1413	δCH_2(C8)
1385s	1390w			1408	δCH_2(C8)	1394	δ_sNH_3,ρ′C12–H29
		1371	ρC12-H29	1371	δ_sCH_3, wagCH_2(C7)	1373	ρC12-H29,wagCH_2(C6)
1368m	1370w	1370	wagCH_2(C7) wagCH_2(C8)	1371	ρ′C4–H15	1372	wagCH_2(C8)
				1367	ρ′C3–H14	1366	wagCH_2(C11)
		1362	ρ′C3–H14	1365	δ_sCH_3, wagCH_2(C8)	1364	ρ′C4–H15
1357sh		1360	wagCH_2(C10)	1361	wagCH_2(C10)	1362	δ_sCH_3
	1354w	1353	wagCH_2(C9)			1353	wagCH_2(C9)
		1345	wagCH_2(C11) ρC5-H16	1352	wagCH_2(C11)	1348	wagCH_2(C11), ρC4-H15
1337w	1338w	1339	δ_sCH_3	1351	ρ′C12–H29	1334	ρC12-H29
1337w	1338w	1331	ρ′C12–H29 ρC12-H29	1332	wagCH_2(C9)		
	1322w	1328	ρ′C4–H15	1329	ρC12-H29 wagCH_2(C6)	1329	wagCH_2(C10),ρ′C5–H16
	1316w	1318	τR_2 (A1), wagCH_2(C7)	1324	wagCH_2(C7)	1322	wagCH_2(C7)
1313w		1314	wagCH_2(C6)	1317	τR_1 (A3)	1317	wagCH_2(C6)
1289w	1292w	1300	ρC4-H15,ρC3-H14	1302	ρC4-H15	1305	ρC3-H14

(*continued on next page*)

Table 6 (*continued*)

Experimental[c]		SQM[b]	Free base	SQM[b]	Cationic	SQM[b]	Hydrochloride
IR	Ra		Assignment[a]		Assignment[a]		Assignment[a]
		1274	ρCH_2(C9)	1282	ρCH_2(C6)	1278	ρCH_2(C8)
		1272	ρCH_2(C7)	1275	ρCH_2(C9), ρCH_2(C8)	1275	ρCH_2(C6),ρCH_2(C11)
1265w	1266m	1270	ρCH_2(C11) ρCH_2(C6)	1272	ρCH_2(C10), ρCH_2(C7)	1272	ρCH_2(C7)
1261w	1260m	1253	τR_2 (A1), τR_1 (A2)	1252	τR_1 (A1),τR_1 (A2)	1250	τR_1 (A1)
	1250sh	1245	τR_2 (A1)			1245	τR_1 (A2),ρCH_2(C7)
1205m	1207s	1220	ρNH_2, ρCH_2(C8)	1250	τR_1 (A3)	1208	$\rho' NH_3$, $\rho' CH_3$
	1191vs			1198	ρC3-H14	1194	τR_1 (A1)
1185m	1181sh	1183	τR_1 (A2), ρCH_2(C10)	1189	ρC5-H16	1182	ρC5-H16
1179sh	1173sh	1175	τR_2 (A1), ρC4-H15	1171	$\rho' CH_3$, δC13C12N1		
1141w	1141w					1142	$\nu_a NH_3$
	1125w			1124	ρCH_2(C7)		
	1117sh	1118	ρCH_3	1123	ρCH_2(C8), ρ′C5–H16	1119	ρCH_3,νC2-C12
	1113w	1113	ρ′C5–H16	1112	ρCH_2(C10) ρCH_2(C11),ρCH_2(C9)	1117	ρ′C3–H14
1102sh	1103w	1106	ρCH_2(C10)			1108	ρCH_2(C10), ρCH_2(C9)
1086w	1096m	1090	τR_2 (A1), τR_1 (A2)	1091	τR_1 (A1), τR_1 (A3)		
1070m	1074w	1071	τR_1 (A3)			1072	τR_1 (A3)
1062sh	1060sh	1058	τR_1 (A1)	1063	τR_1 (A1), τR_2 (A3)	1062	τR_1 (A1)
		1055	τR_2 (A1), τR_2 (A1)	1056	τR_1 (A1), τR_2 (A1)	1058	τR_2 (A1), τR_1 (A3)
1044sh	1036w			1038	τR_1 (A2)	1047	τR_1 (A2), τR_2 (A3)
1034w		1032	τR_1 (A2)	1031	τR_1 (A1), τR_1 (A3)		
	1000sh	1009	νC4-C11,νC5-C11	1013	νC3-C10, νC4-C11	1010	νC5-C11
994sh	996sh	1007	νC3-C9	999	νC5-C8, νC4-C7	1007	νC3-C9
988w	990m	998	νC5-C8, νC3-C6	997	νC3-C6	1005	νC3-C6, νC5-C8
982sh	984m	976	νC12-C13, ρCH_3			976	$\nu_a NH_3$,τR_2 (A1)
964w	968s	954	τR_2 (A1),τR_2 (A2)	953	τR_2 (A1), τR_2 (A2)	962	τR_2 (A1)
950sh	952w					941	τR_2 (A1), $\nu_a NH_3$
924vw	934w	929	τR_3 (A2),τR_2 (A3)	922	τR_3 (A2)	927	$\nu_a NH_3$,$\nu_s NH_3$
		924	τR_2 (A3), τR_3 (A1)	921	ρNH_3, ρCH_3	924	τR_3 (A2),$\nu_a NH_3$
	910w			919	τR_2 (A3), τR_3 (A1)	919	$\nu_a NH_3$,τR_2 (A3)
905vw		909	νC3-C10, νC5-C8	908	νC3-C10, νC3-C9	905	νC4-C7
		902	νC3-C6	906	νC5-C11	901	νC4-C11, νC4-C9
875vw	881w	893	νC4-C7	896	$\rho' NH_3$ νC12-C13		
839vw	845w			844	νC2-C12	866	$\nu_a NH_3$,$\nu_s NH_3$
		827	νC2-C12				
		821	wagNH_2, νC12-N1 $\rho' CH_3$			817	νC12-N1,νC12-C13
807w	810vw	810	τwCH_2(C10) τwCH_2(C8)	808	τwCH_2(C9) τwCH_2(C7)	810	τwCH_2(C9) τwCH_2(C10)
807w	810vw	809	τwCH_2(C9) τwCH_2(C11)	806	τwCH_2(C11) τwCH_2(C10)	806	τwCH_2(C11)
807w	810vw	807	τwCH_2(C7) τwCH_2(C6)	802	τwCH_2(C6) τwCH_2(C8)		
		785	τR_2 (A3), νC4-C11	786	τR_2 (A3),νC4-C11	801	τwCH_2(C6), τwCH_2(C7) τwCH_2(C8)
765w	771vs	782	νC5-C10	783	νC4-C9, νC5-C10	783	τR_2 (A3), νC4-C11
	767sh			756	νC12-N1	781	τR_3 (A1), τR_3 (A2)
687w	696vs	743	νC4-C9	738	νC4-C11	744	νC3-C10, νC5-C10
662vw	696vs	678	νC2-C6, νC2-C8 νC2-C7,βR_2 (A3)	670	νC2-C6 νC2-C7 νC2-C8	674	νC2-C6,νC2-C7, νC2-C8
634vw	642w	630	βR_3 (A3)	626	τR_3 (A2), τR_2 (A1)	627	τR_2 (A3), τR_3 (A2)
614vw		629	τR_3 (A2), τR_2 (A1)	625	βR_3 (A3)	625	τR_3 (A1), βR_3 (A3)
576m	582w	584	δC2C12N1 δC2C12C13			581	δC2C12N1, δC2C12C13
548vw				553	δC2C12C13, δC2C12N1		
487m	495m	480	δC13C12N1			480	δC13C12N1
451m	451w	447	τR_2 (A1), τR_1 (A3)	463	τR_2 (A1) τR_2 (A2)	455	νH33-Cl36
	439w	433	τR_2 (A1), τR_2 (A1)	434	βR_2 (A3)		
427w	421w	428	τR_1 (A2)	422	τR_1 (A2)	433	τR_1 (A3),τR_2 (A1)
		419	τR_2 (A1), τR_1 (A3)	421	τR_1 (A1)	421	τR_1 (A1)
411s				415	τR_1 (A3)	413	τR_1 (A2)
411s		411	βR_3 (A2)			410	τR_2 (A3), βR_3 (A3)
	405w			404	βR_3 (A2)	406	βR_3 (A2), βR_2 (A3)
	389w	390	τR_2 (A1)	384	τR_2 (A1)	376	τR_2 (A1)
	389w	390				374	τR_1 (A3),τR_2 (A1)
	347w	342	τR_2 (A2)				

(*continued on next page*)

Table 6 (*continued*)

Experimental[c]		SQM[b]	Free base	SQM[b]	Cationic	SQM[b]	Hydrochloride
IR	Ra		Assignment[a]		Assignment[a]		Assignment[a]
	320sh	310	τR_2 (A3)	334	δC2C12N1	332	τR_2 (A2)
	306m	304	τR_3 (A2),τR_3 (A1)	302	τR_2 (A1), τR_2 (A3)	303	τR_2 (A1), τR_3 (A1)
	302sh	300	τR_2 (A2),βR_3 (A2)	297	τR_3 (A2)		
	292sh			293	τR_2 (A3)	293	τR_3 (A2) τR_2 (A3)
	240sh	235	$\tau_w NH_2$			243	τR_2 (A1), τR_2 (A3)
	192m	207	$\tau_w CH_3$	215	$\tau_w CH_3$	219	$\tau_w CH_3$
	188sh			186	τR_3 (A3),ρ′C12–N1	182	τR_3 (A),ρ′C12–N1
	176m	179	τR_3 (A3),ρ′C12–N1	178	ρC12-N1		
	166m	174	ρC12-N1	171	$\tau_w NH_3$		
	154w					150	ρC12-N1
		61	τC12-C2			76	ρNH_3, τN1-H33
				52	τC12-C2, $\tau_w CH_3$		
						44	τC12-C2
						31	$\tau_w NH_3$, δN1H33Cl36

Abbreviations: ν, stretching; wag, wagging; τ, torsion; ρ, rocking; τw, twisting; δ, deformation; a, antisymmetric; s, symmetric; a, antisymmetric; s, symmetric (A_1), Ring 1 (A_2), Ring 2 (A_3), Ring 3.

[a] This work.

[b] From scaled quantum mechanics force field B3LYP/6–311++G** method.

[c] From Ref [32].

Table 7. Scaled internal force constants for the free base, cationic and hydrochloride rimantadine species in gas phase compared with the corresponding to amantadine by using the B3LYP/6–311++G** method.

Force constants	Rimantadine[a]			Adamantadine[b]		
	Free base	Cationic	Hydrochloride	Free base	Cationic	Hydrochloride
f(νN-H)	6.42	6.12	4.81	6.31	6.08	4.99
f(νC-N)	4.32	2.81	3.81	4.38	2.54	4.78
f(νC-H)	4.53	4.72	4.66	4.63	4.75	4.70
$f(\nu C\text{-}C)_R$	4.39	4.39	439	4.50	4.50	6.11
$f(\nu CH_2)$	4.64	4.65	4.65	4.64	4.69	4.71
$f(\delta CH_2)$	0.71	0.71	0.73	0.71	0.71	0.73

Units are mdyn $Å^{-1}$ for stretching and mdyn Å rad^{-2} for angle deformations.

[a] This work.

[b] From Ref [14].

5. NMR study

The GIAO and hybrid B3LYP/6–311++G** methods were employed to calculate the ^{1}H- and ^{13}C-NMR chemical shifts of the three species of rimantadine in aqueous solution [41]. Comparisons of those chemical shifts with the corresponding experimental for the HCl species in $CDCl_3$ are presented in Tables 8 and 9 [52]. The differences between experimental and theoretical values are presented in terms of RMSD values. Note that in general, the ^{1}H and ^{13}C nucleus values predicted by calculations for the three species are overestimated, in relation to the experimental ones. The evaluation of results show that the ^{1}H nucleus show a better correlation with RMSD values between 0.144 and 0.098 ppm while the RMSD values of the ^{13}C nucleus are between 4.73 and 4.25 ppm. The proximities among the results for the three species suggest the presence of three species in solution. Obviously, the different media used in the calculations (aqueous solution) could justify the slight differences in the RMSD values performed because the experimental spectrum was obtained in $CDCl_3$. However, these good correlations predicted in solution support the qualities of optimized structures by using the B3LYP/6–311++G** method.

6. Electronic spectrum

Time-dependent DFT calculations (TD-DFT) combined with the B3LYP/6–311++G** method were used to predict the UV-visible spectra of the three species of rimantadine in aqueous solution by using the Gaussian 09 program [22]. The predicted UV spectra of three species are compared in Figure 6 with the experimental reported by Odnovorov et al. for the HCl of rimantadine in ethanol solution [47]. In the experimental spectrum of Figure 6a is observed two bands, one intense at 230 nm and the other weak at 256 nm while in the predicted spectra for the three species are observed two bands with different intensities. Thus, in the absorption spectrum of FB can be seen a peak maximum at c. a. 144 nm and a minimum at 176 nm, as in the same species of amantadine [14]. These bands cannot be experimentally observed because the UV spectrum only can be recorded from 200 nm. The CA species shows two bands, a weak at 162 nm and other intense at 192 nm. The HCl species show two bands, a weak at 210 nm and other intense at 255 nm, respectively, as in the CA species but both bands with different intensities and wavelengths. Note that the predicted spectrum for the HCl species presents two bands practically in the same positions than the

Table 8. Observed and calculated ^{1}H chemical shifts (δ in ppm) for the three species of rimantadine in aqueous solutions by using the 6–311++G** method.

H atom	B3LYP/6–311++G** Method[a]			Exp[a]
	Free base	Cation	Hydrochloride	
14-H	1.79	1.97	1.88	1.99
15-H	1.80	1.93	1.89	1.99
16-H	1.80	1.95	1.94	1.99
17-H	1.48	1.74	1.68	1.51
18-H	1.78	1.35	1.24	1.51
19-H	1.21	1.41	1.36	1.51
20-H	1.68	1.79	1.66	1.51
21-H	1.76	1.60	1.62	1.51
22-H	1.25	1.56	1.43	1.51
23-H	1.69	1.76	1.79	1.71
24-H	1.61	1.67	1.71	1.63
25-H	1.60	1.63	1.64	1.63
26-H	1.70	1.79	1.81	1.71
27-H	1.71	1.79	1.79	1.71
28-H	1.60	1.67	1.67	1.63
29-H	2.63	3.13	2.84	2.40
30-H	1.14	1.62	1.32	0.97
31-H	0.85	1.27	1.05	0.97
32-H	0.63	4.16	1.19	0.97
33-H	0.39	4.92	10.54	1.04
34-H	1.05	1.97	4.11	1.04
RMSD[a]	**0.144**	**0.094**	**0.098**	

[b]From Ref [52].
[a] This work GIAO/B3LYP/6–311++G** Ref. to TMS.

Table 9. Observed and calculated ^{13}C chemical shifts (δ in ppm) for the three species of rimantadine in aqueous solutions by using the 6–311++G** method.

C atoms	B3LYP/6–311++G** Method[a]			Exp[b]
	Free base	Cation	Hydrochloride	
2-C	40.77	39.80	39.20	35.90
3-C	34.36	33.57	33.02	28.55
4-C	34.49	33.64	33.40	28.55
5-C	34.51	33.89	33.66	28.55
6-C	35.81	34.76	35.41	38.16
7-C	43.60	41.77	41.36	38.16
8-C	43.07	41.63	43.47	38.16
9-C	41.08	39.79	40.15	37.35
10-C	40.65	39.64	39.65	37.35
11-C	40.20	39.12	39.73	37.35
12-C	60.19	66.22	62.77	55.85
13-C	16.07	13.07	12.08	16.97
RMSD[a]	**4.47**	**4.73**	**4.25**	

[a] This work GIAO/B3LYP/6–311++G** Ref, to TMS.
[b] From Ref [52].

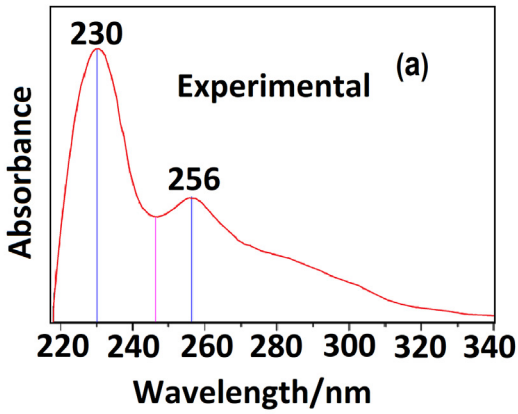

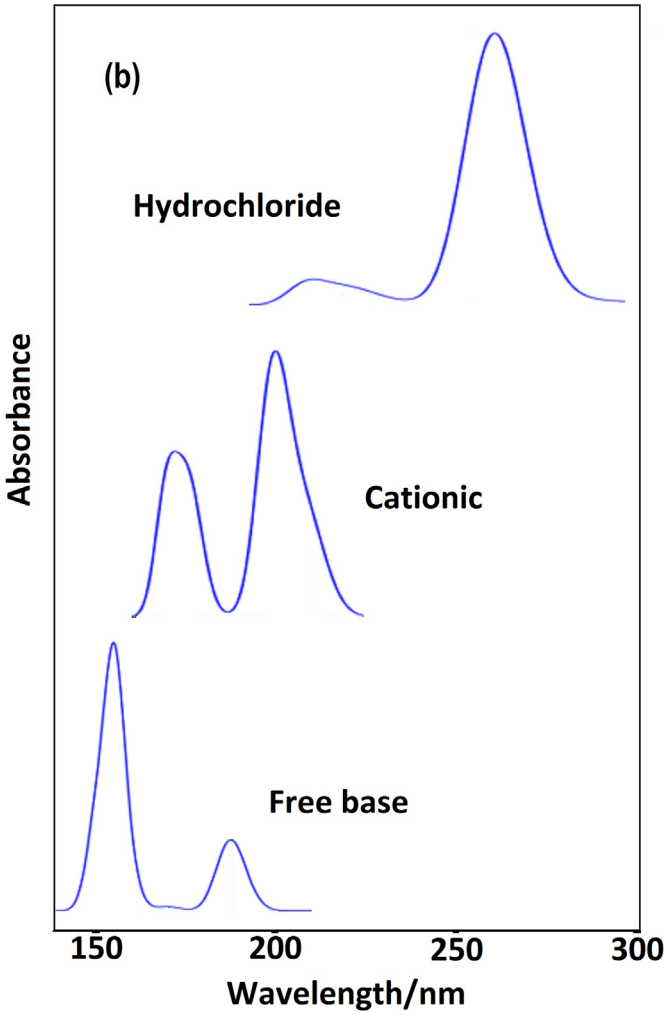

Figure 6. Experimental available electronic spectrum of hydrochloride rimantadine in ethanol solution [47] compared with those predicted for the three species in aqueous solution by using the B3LYP/6–311++G** method.

experimental one although with different intensities, as expected because it is the same species. The absorption bands observed in the FB and HCl species are attributed to the σ→σ* and n→σ* transitions predicted by NBO analyses but for the CA species the first transitions are very weak while the second one are not observed. In order to explain the differences in the intensities of bands, the character of the molecular orbitals (LUMO and HOMO) in three species of rimantadine were predicted with the density of states (DOS). Thus, from DOS spectra presented in Figure S5 we can see two peaks for the CA and HCl species in solution while only one for the FB. In water, the FB is protonated as CA while probably part of the HCl species is also as CA one. Then, the band predicted in the CA species in 192 nm is in agreement with the band predicted in the HCl species at 210 nm and with the experimental at 230 nm. This way, the band at 230 nm will be increased by the CA species while the band at 255 of HCl species decreases due to that a part of this form is as CA one. Besides, the differences observed in the intensities of absorption bands could be explained with the aid of electronic circular dichroism (ECD) spectra predicted for each species of rimantadine in aqueous solution at the same level of theory. These spectra are shown in Figure S6 and

clearly, the figure shows that the FB and the CA species present positive Cotton effects (CE) while in the HCl species this effect is negative justifying this way different conformations and intensities of bands in this form of rimantadine. Moreover, the presence of this negative effect in the HCl species could also justify the different orientation and direction of dipole moment vector of this species, in relation to the other ones.

7. Conclusions

In this work, structural and vibrational properties of FB, CA and HCl species of antiviral rimantadine were predicted combining hybrid B3LYP/6–311++G** calculations with the scaled quantum force field (SQMFF) methodology. Here, the harmonic force fields and scaled force constants of three species in gas phase and in aqueous solution have been computed using normal internal coordinates and scaling factors. Good correlations were obtained comparing the predicted IR, Raman, ^{1}H– ^{13}C-NMR and UV spectra of three species with the corresponding experimental ones, suggesting the presence of all them in the solid phase and in solution. The main force constants of three species have evidenced lower values than the corresponding to antiviral amantadine. Positive Mulliken charge on N1 atom of HCl species in aqueous solution evidence the ionic character of N1–H33···Cl36 bond indicating that this species is as CA one. Rimantadine presents higher solvation energies in water than other antiviral species, such as chloroquin, niclosamide, cidofovir and brincidofovir. The FB and HCl species of rimantadine are slightly less reactive than the corresponding to amantadine while the opposite is observed for the CA species. The predicted ECD spectra for the FB and CA species show positive Cotton effect different from the negative observed for the HCl one. These different behaviours of three species of rimantadine could probably explain the differences observed in the intensities of bands predicted in the UV spectra of these species. Here, complete vibrational assignments of 96, 99 and 102 vibration modes expected for FB, CA and HCl species have been reported combining the hybrid B3LYP/6–311++G** method with the SQMFF methodology.

Declarations

Author contribution statement

Maximiliano A. Iramain: Performed experiments; Contributed reagents, materials, analysis tools or data.

José Ruiz Hidalgo, Tom Sundius: Performed experiments; Analyzed and interpreted the data.

Silvia Antonia Brandán: Conceived and designed the experiments; Analyzed and interpreted the data; Contributed reagents, materials, analysis tools or data; Wrote the paper.

Funding statement

This work was supported by Consejo de Investigaciones, Universidad Nacional de Tucumán (CIUNT Project No. 26/D608).

Data availability statement

Data will be made available on request.

Declaration of interests statement

The authors declare the following conflict of interest: Silvia Antonia Brandán is part of the Editorial Board for Heliyon Chemistry.

Additional information

Supplementary content related to this article has been published online at https://doi.org/10.1016/j.heliyon.2022.e10102.

Acknowledgements

This work was supported by Consejo de Investigaciones Universidad Nacional de Tucumán (CIUNT) Project No. 26/D608.

References

[1] R.A. Rudyk, M.A. Checa, C.A.N. Catalán, S.A. Brandán, Structural, FT-IR, FT-Raman and ECD studies on the FB, CA and hydrobromide species of scopolamine alkaloid, J. Mol. Struct. 1180 (2019) 603–617.
[2] D. Romani, I. Salas Tonello, S.A. Brandán, Influence of atomic bonds on the properties of the laxative drug sodium picosulphate, Heliyon 2 (2016), e00190.
[3] M.E. Manzur, S.A. Brandán, S(-) and R(+) species derived from Antihistaminic promethazine agent: structural and vibrational studies, Heliyon 5 (2019), e02322.
[4] A. Sagaama, S.A. Brandán, T. Ben Issa, N. Issaoui, Searching potential antiviral candidates for the treatment of the 2019 novel coronavirus based on DFT calculations and molecular docking, Heliyon 6 (2020), e04640.
[5] P. Pulay, G. Fogarasi, G. Pongor, J.E. Boggs, A. Vargha, Combination of theoretical ab initio and experimental information to obtain reliable harmonic force constants. Scaled quantum mechanical (QM) force fields for glyoxal, acrolein, butadiene, formaldehyde, and ethylene, J. Am. Chem. Soc. 105 (1983) 7073.
[6] E. De Clercq, Antiviral drugs: current state of the art, J. Clin. Virol. 22 (2001) 73–89.
[7] G. Zoidis, N. Kolocouris, G.B. Foscolos, A. Kolocouris, G. Fytas, P. Karayannis, E. Padalko, J. Neyts, E. De Clercq, Are the 2-isomers of the drug rimantadine active anti-influenza A agents? Antivir. Chem. Chemother 14 (2003) 153–164.
[8] E. De Clercq, Antiviral drugs in current clinical use, J. Clin. Virol. 30 (2004) 115–133.
[9] G. Zoidis, C. Fytas, I. Papanastasiou, G.B. Foscolos, G. Fytas, E. Padalko, E. De Clercq, L. Naesens, J. Neyts, N. Kolocouris, Heterocyclic rimantadine analogues with antiviral activity, Bioorg. Med. Chem. 14 (2006) 3341–3348.
[10] A.V. Titova, A.P. Arzamastsev, S.V. Gretskii, Structure of chemical compounds, methods of analysis and process control analysis of rimantadine hydrochloride by near-ir spectroscopy, Pharmaceut. Chem. J. 43 (9) (2009) 534–537.
[11] M.G. Alves Galvão, M.A. Rocha Crispino Santos, A.J.L. Alves da Cunha, Amantadine and rimantadine for influenza A in children and the elderly (Review), Cochrane Database Syst. Rev. 11 (2014). **Art. No: CD002745.** Published by John Wiley & Sons, Ltd (2014).
[12] B.-M. Liu, P. Ma, X. Wang, Y.-M. Kong, L.-P. Zhang, B. Liu, Synthesis of three rimantadine Schiff bases and their biological effects on Serum Albumin, Iran. J. Pharm. Res. (IJPR) 13 (4) (2014) 1183–1190.
[13] J. Mamatha, N. Devanna, Development and validation of a RP-HPLC method for the analysis of rimantadine hydrochloride in medicinal form, Rasayan J. Chem. 11 (1) (2018) 300–306.
[14] S.A. Brandán, Normal internal coordinates Force fields and vibrational study of Species Derived from Antiviral adamantadine, Int. J. Quant. Chem. 121 (2) (2021), e26425.
[15] G. Rauhut, P. Pulay, Transferable scaling factors for density functional derived vibrational force fields, J. Phys. Chem. 99 (1995) 3093–3100.
[16] T. Sundius, Scaling of ab-initio force fields by MOLVIB, Vib. Spectrosc. 29 (2002) 89–95.
[17] D. Romani, S.A. Brandán, Effect of the side chain on the properties from cidofovir to brincidofovir, an experimental antiviral drug against to Ebola virus disease, Arab. J. Chem. 12 (2019) 2959–2972.
[18] D. Romani, O. Noureddine, N. Issaoui, S.A. Brandán, Properties, reactivities and molecular docking of potential antiviral to treatment of COVID-19 niclosamide in different media, Biointerface Research in Applied Chemistry 10 (6) (2020) 7295–7328.
[19] E. Romano, N. Issaoui, M.E. Manzur, S.A. Brandán, Properties and Molecular docking of Antiviral to COVID-19 Chloroquine combining DFT calculations with SQMFF approach, International Journal of Current Advanced Research 9 (8A) (2020) 22862–22876.
[20] A.B. Nielsen, A.J. Holder, Gauss View 5.0, User's Reference, GAUSSIAN Inc., Pittsburgh, PA, 2008.
[21] A.D. Becke, Density-functional exchange-energy approximation with correct asymptotic behavior, Phys. Rev. A38 (1988) 3098–3100.
[22] C. Lee, W. Yang, R.G. Parr, Development of the Colle-Salvetti correlation-energy formula into a functional of the electron density, Phys. Rev. B37 (1988) 785–789.
[23] M.J. Frisch, et al., Gaussian, Inc., Wallingford CT, 2009.
[24] S. Miertus, E. Scrocco, J. Tomasi, Electrostatic interaction of a solute with a continuum, Chem. Phys. 55 (1981) 117–129.
[25] J. Tomasi, J. Persico, Molecular interactions in solution: an Overview of methods based on continous distributions of the solvent, Chem. Rev. 94 (1994) 2027–2094.
[26] A.V. Marenich, C.J. Cramer, D.G. Truhlar, Universal solvation model based on solute electron density and a continuum model of the solvent defined by the bulk dielectric constant and atomic surface tensions, J. Phys. Chem. B113 (2009) 6378–6396.
[27] P. Ugliengo, MOLDRAW Program, University of Torino, Dipartimento Chimica IFM, Torino, Italy, 1998.
[28] E.D. Glendening, J.K. Badenhoop, A.D. Reed, J.E. Carpenter, F. Weinhold, NBO 3.1; Theoretical Chemistry Institute, University of Wisconsin, Madison, WI, 1996.
[29] R.F.W. Bader, Atoms in Molecules, A Quantum Theory, Oxford University Press, Oxford, 1990, ISBN 0198558651.

[30] F. Biegler-Köning, J. Schönbohm, D. Bayles, AIM 2000; A program to Analyze and Visualize atoms in molecules, J. Comput. Chem. 22 (2001) 545.
[31] B.H. Besler, K.M. Merz Jr., P.A. Kollman, Atomic charges derived from semiempirical methods, J. Comput. Chem. 11 (1990) 431–439.
[32] T. Koopmans, Über die Zuordnung von Wellenfunktionen und Eigenwertenzu den Einzelnen Elektronen Eines Atoms, Physica 1 (1934) 104–113.
[33] J.P. Perdew, R.G. Parr, M. Levy, J.L. Balduz, Density-functional theory for Fractional Particle number: Derivative Discontinuities of the energy, Phys. Rev. Lett. 49 (23) (1982) 1691–1694.
[34] J.F. Janak, Proof that ∂E/∂ni=εin density-functional theory, Phys. Rev. B 18 (12) (1978) 7165–7168.
[35] J.P. Perdew, M. Levy, Physical content of the Exact Kohn-Sham orbital energies: band gaps and Derivative Discontinuities, Phys. Rev. Lett. 51 (20) (1983) 1884–1887.
[36] R.G. Parr, R.G. Pearson, "Absolute hardness: companion parameter to absolute electronegativity", J. Am. Chem. Soc. 105 (1983) 7512–7516.
[37] R.G. Pearson, Absolute electronegativity and hardness correlated with molecular orbital theory, Proc. Natl. Acad. Sci. U.S.A. 83 (1986) 8440–8441.
[38] R.G. Parr, L.V. Szentpaly, S. Liu, Electrophilicity index, J. Am. Chem. Soc. 121 (1999) 1922–1924.
[39] Available from Web page. https://spectrabase.com/spectrum.
[40] G. Keresztury, S. Holly, G. Besenyei, J. Varga, A.Y. Wang, J.R. Durig, Vibrational spectra of monothiocarbamates-II. IR and Raman spectra, vibrational assignment, conformational analysis and ab initio calculations of S-methyl-N,N-dimethylthiocarbamate Spectrochim, Acta 49A (1993) 2007–2026.
[41] R. Ditchfield, Self-consistent perturbation theory of diamagnetism. I. A gage-invariant LCAO (linear combination of atomic orbitals) method for NMR chemical shifts, Mol. Phys. 27 (1974) 714–722.
[42] M.E. Casida, C. Jamorski, K.C. Casida, D.R. Salahub, Molecular excitation energies to high-lying bound states from time-dependent density-functional response theory: Characterization and correction of the time-dependent local density approximation ionization threshold, J. Chem. Phys. 108 (1998) 4439–4449.
[43] G. Scalmani, M.J. Frisch, B. Mennucci, J. Tomasi, R. Cammi, V. Barone, Geometries and properties of excited states in the gas phase and in solution: theory and application of a time-dependent density functional theory polarizable continuum model, J. Chem. Phys. 124 (9) (2006) 1–15.
[44] C. Van Caillie, R.D. Amos, Geometric derivatives of excitation energies using SCF and DFT, Chem. Phys. Lett. 308 (1999) 249–255.
[45] C. Adamo, D. Jacquemin, The calculations of excited-state properties with time-dependent density functional theory, Chem. Soc. Rev. 42 (2013) 845–856.
[46] R. Importa, C. Ferrante, R. Bozioc, V. Barone, The polarizability in solution of tetra-phenyl-porphyrin derivatives in their excited electronic states: a PCM/TD-DFT study, Phys. Chem. Chem. Phys. 11 (2009) 4664–4673.
[47] A.I. Odnovorov, T.V. Grebennikova, T.V. Pleteneva, T.M. Garaev, E.V. Uspenskaya, N.A. Khodorovich, O.V. Levitskaya, A.M. Koldina, Physicochemical properties and biological activity of the new antiviral substance, Int. J. Appl. Pharm. 12 (4) (2020) 2–6.
[48] Anatoly Mishnev, Dmitrijs Stepanovs, Crystal structure explains Crystal Habit for the antiviral drug rimantadine hydrochloride, Z. Naturforsch 69b (2014) 823–828.
[49] C.F. Matta, Modeling biophysical and biological properties from the characteristics of the molecular electron density, electron localization and delocalization matrices, and the electrostatic potential, J. Chem. Comp. 35 (2014) 1165–1198.
[50] D.F. Veber, S.R. Johnson, H.-Y. Cheng, R. Brian, K.W. Ward, K.D. Kopple, Molecular Properties that influence the oral bioavailability of drug candidates, J. Med. Chem. 45 (2002) 2615–2623.
[51] C.A. Lipinski, F. Lombardo, B.W. Dominy, P.J. Feeney, Experimental and computational approaches to estimate solubility and permeability in drug discovery and development setting, Adv. Drug Deliv. Rev. 46 (2001) 3–26.
[52] Available from Web page. http://drugapprovalsint.com/rimantadine-hydrochloride/.